

Complex transport behaviors of rectangular graphene quantum dots subject to mechanical vibrations

This content has been downloaded from IOPscience. Please scroll down to see the full text.

2016 EPL 114 47006

(<http://iopscience.iop.org/0295-5075/114/4/47006>)

View the [table of contents for this issue](#), or go to the [journal homepage](#) for more

Download details:

IP Address: 129.219.51.205

This content was downloaded on 05/08/2016 at 23:08

Please note that [terms and conditions apply](#).

Complex transport behaviors of rectangular graphene quantum dots subject to mechanical vibrations

MENGKE XU^{1(a)}, YISEN WANG^{1(a)}, RUI BAO¹, LIANG HUANG^{1(b)} and YING-CHENG LAI^{2,3}

¹ School of Physical Science and Technology, and Key Laboratory for Magnetism and Magnetic Materials of MOE, Lanzhou University, Lanzhou, Gansu 730000, China

² School of Electrical, Computer, and Energy Engineering, Arizona State University - Tempe, AZ 85287, USA

³ Department of Physics, Arizona State University - Tempe, AZ 85287, USA

received 29 February 2016; accepted in final form 27 May 2016

published online 16 June 2016

PACS 72.80.Vp – Electronic transport in graphene

PACS 73.23.-b – Electronic transport in mesoscopic systems

Abstract – Graphene-based mechanical resonators have attracted much attention due to their superior elastic properties and extremely low mass density. We investigate the effects of mechanical vibrations on electronic transport through graphene quantum dots, under the physically reasonable assumption that the time scale associated with electronic transport is much shorter than that with mechanical vibration so that, at any given time, an electron “sees” a static but deformed graphene sheet. We find that, besides periodic oscillation in the quantum transmission at the same frequency as that of mechanical vibrations, structures at finer scales can emerge as an intermediate state, which may lead to spurious higher-frequency components in the current through the device.

Copyright © EPLA, 2016

Introduction. – In the past decade graphene has attracted much attention due to its peculiar electronic and mechanical properties [1–4]. Because of its superior elastic quality [5] and the truly two-dimensional nature (*e.g.*, a single layer of atoms), graphene has been recognized as an excellent candidate material for developing high-frequency and high-quality factor nanomechanical resonators [6–10]. Both optical [6,7] and electrical [8–10] readouts have been exploited for the detection of mechanical motions, with the latter being more compatible with microelectronic applications. In the electrical readout schemes, it is assumed that the mechanical vibrations would result in an AC current of the same frequency, and thus can be readily identified in a current analysis. At the present our understanding of how mechanical vibrations affect electronic transport is incomplete, in spite of works on the electronic and/or magnetic responses from rippled graphene [11–13] or graphene under strain [14,15].

A different approach to treating vibrating graphene is to consider joint transport of coupled phonons and electrons [16–18], where the mechanical part is regarded as contributing to thermally excited phonons. However, direct treatment to understand the effects of mechanical

vibrations on electronic transport is still lacking, which becomes an urgent issue in the development of graphene-based nanoelectromechanical devices.

In this paper, we focus on the effects of mechanical vibrations on electronic transmission in a single graphene sheet. For a mechanical resonator, the sheet is typically under external driving and vibrates periodically. In general the mechanical vibration may bring ripples along the graphene edges [19,20]. For simplicity, we consider a quantum-dot system consisting of a rectangular graphene sheet with all boundaries fixed similar to their circular counterparts [7,21,22], which moves freely starting from an initial deformation in the lowest vibrational mode. Although in realistic cases typically only one parallel side of the rectangle are fixed while the other two boundaries are free to move [6,8–10], we expect that the vibrational effects to the electron transport should be similar to our results. For free vibration, linear interactions in graphene are the dominant contributing factor to periodic motion. Nonlinear interactions can be included to yield more complex mechanical and electronic behaviors. Specifically, our approach is the following. We note that, for a fixed Fermi energy, the electronic motion is orders of magnitude faster than the mechanical motion. Thus, at any time, the graphene quantum dot can be regarded as static but deformed. The hopping energy between atoms can

^(a)These authors contributed equally.

^(b)E-mail: huangl@lzu.edu.cn

then be reevaluated, using the deformation at the time as input. The new set of hopping energies can be utilized to calculate the quantum transmission, yielding a time-dependent transmission curve. Our computations indicate that the transmission patterns can be quite complex. For small-amplitude vibrations, each transmission peak for the static graphene is extended into a transmission band, which bends downwards as the graphene sheet moves away from the flat equilibrium. As the amplitude is increased slightly, the bands are expanded into plateaus, leading to transmission enhancement. However, as the amplitude becomes larger, due to inhomogeneity in the spatial distribution of the hopping energies, finer structures of the bands emerge. In particular, the bands can cross each other, leading to complex transmission patterns. When nonlinear interactions are taken into account, the vibrations are no longer periodic: higher-order modes can be excited. In this case, due to enhanced inhomogeneity, the bands are braided into a net of high transmission paths. As a result, although periodic mechanical motions would yield periodic variation in the transmission, the fine structures in the intermediate state can result in spurious high frequencies, *e.g.*, in a current analysis. Our findings can be practically useful for developing graphene-based nanoelectromechanical devices.

Model. — Our vibrating graphene system is shown schematically in fig. 1. It is a rectangular graphene quantum dot with fixed boundaries, where the left and right narrow leads are made of graphene ribbon. For simplicity, we focus on vibrations in the z -direction (normal to the graphene plane). To model the mechanical motion of graphene, we use the valence force field model [23–26]:

$$\begin{aligned} U_{sp^2} = & \frac{1}{2} \sum_{i=1}^N \sum_{j=i'sn.n.}^3 \frac{\alpha}{4a_0^2} (\vec{r}_{ij}^2 - a_0^2)^2 \\ & + \sum_{i=1}^N \sum_{\substack{j < k \\ j,k=i'sn.n.}} \frac{\beta}{a_0^2} (\vec{r}_{ij} \cdot \vec{r}_{ik} + \frac{1}{2} a_0^2)^2 \\ & + \sum_{i=1}^N \gamma \vec{D}_i \cdot \vec{D}_i, \end{aligned} \quad (1)$$

where N is the total number of the atoms, i is the atom index and j and k are indices labeling the nearest neighboring atoms. The three bond vectors \vec{r}_{ij} ($j = 1, 2, 3$) connect atom i to its nearest neighbors. The parameters α , β and γ are constant and have the values of 155.9 J/m^2 , 25.5 J/m^2 , 7.4 J/m^2 , respectively. They have the same dimension as the coefficient of stiffness. The equilibrium bond length is $a_0 = 1.420 \text{ \AA}$ and $\vec{D}_i = \sum_{j=i'sn.n.} \vec{r}_{ij}$ is the dangling bond vector, where “n.n.” denotes the set of nearest neighbors. The first two terms in eq. (1) represent the energy cost necessary to change the length and angle between the covalent C-C bonds, and the last term represents the energy needed to change the angle between

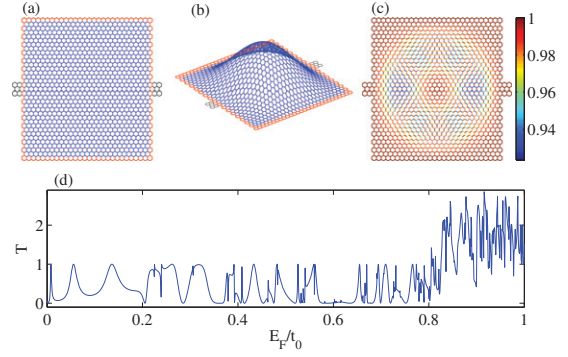


Fig. 1: (Color online) (a) Rectangular graphene quantum dot of fixed boundaries (red/light grey). The leads are semi-infinite graphene ribbons. The dot is 6.9 nm (length) by 7.5 nm (width), and the width of the lead is 0.71 nm . (b) Profile of initial deformation in the lowest vibrational mode. (c) Profile of hopping energies (in units of t_0) under the same deformation for $\eta_0 = 0.07$. The maximum bond elongation is 7.43% . (d) The transmission coefficient *vs.* the Fermi energy for the flat graphene quantum dot (a).

the p_z -orbitals, which are approximately normal to the graphene surface.

To calculate the eigenmodes associated with mechanical vibrations, we neglect nonlinear interactions and keep only the linear term¹. Since the first mode is relatively much easier to be excited, and it is the most common mode used in graphene resonator application, we assume the initial perturbation is on this particular mode to demonstrate the complex behaviors of the transmission under vibration. Perturbations on other modes show qualitatively similar behavior. The system is then perturbed with a deformation of the shape of the lowest vibration mode, and is allowed to move freely under the force field. We consider two cases, where the force field is given by (a) only the third potential term in eq. (1), which is linear under small deformations, and (b) all three terms in eq. (1) to include both linear and nonlinear interactions. At each time step t , from the deformation configuration of the graphene sheet, we calculate the distance $r_{ij}(t)$ between the nearest neighboring atoms i and j and then the hopping energy $t_{ij}(t) = t_0 e^{-3.37(r_{ij}(t)/a_0 - 1)}$ [27–30], where $t_0 \approx 2.8 \text{ eV}$ is the hopping energy between nearest neighbors in the flat graphene [1]. Note that this equation perfectly describes the exponential decrease of the hopping energy with inter-atomic distance, which has been confirmed with *ab initio* calculations [28]. For a full exploration of the three-dimensional motion of graphene, the effect of local rotation of p_z -orbitals [30] should be included. While for small-amplitude vibration, the corresponding

¹By considering the vibration only in the z -direction, the linear term in the U_{sp^2} potential is the third term $U_3 = \sum_{i=1}^N \gamma \vec{D}_i \cdot \vec{D}_i$, and it can be simplified as $\sum_{i=1}^N \gamma (\sum_{j=i'sn.n.} z_j - 3z_i)^2$. Define $V_{mn}^3 = -\frac{\partial^2 U_3}{\partial z_m \partial z_n}$, one can get the matrix V^3 , whose eigenvectors are the vibration eigenmodes.

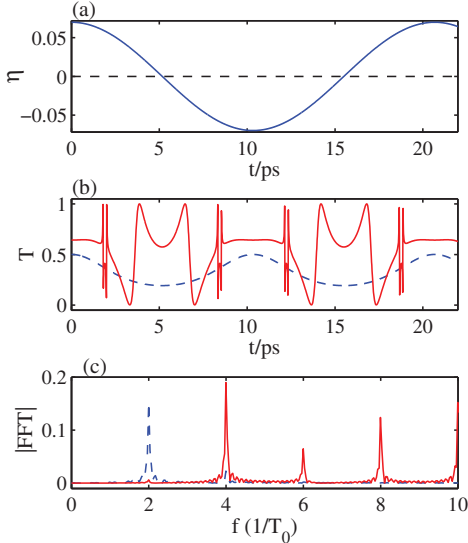


Fig. 2: (Color online) (a) Time evolution of the maximum deformation η , where the initial deformation amplitude is $\eta_0 = 0.07$. (b) The corresponding transmission coefficient T vs. time for $E/t_0 = 0.04$ (dashed curve) and 0.6525 (solid curve). (c) Fourier spectra of the corresponding transmission curves in (b). The frequency is in units of $1/T_0$, with $T_0 = 20.64$ ps being the period of the mechanical vibration. The length of the data for doing the Fourier transform is $20T_0$.

correction is small and can be neglected [31]². With this new set of hopping energies, we obtain a modified tight-binding Hamiltonian, which can be used to calculate the transmission coefficient and the local density of states via the standard Green's function formalism [32,33]. A critical issue of this procedure is the separation of the time scales for the mechanical vibration and the electron motion. The period of the mechanical vibration is around 21 ps (fig. 2). The Fermi velocity of the graphene electron is $v_F = 10^6$ m/s [1]. The length scale of the quantum dot we considered is around 7 nm. If one assumes that the electron passes the quantum dot ballistically, the time scale would be 0.007 ps. For sharp resonances in the transmission curve *vs.* the variation of the Fermi energy, the electron could be trapped in the quantum dot for a much longer time. In this case, the typical energy scale for the resonance is $\Delta E \sim 0.001t_0$, the corresponding time scale is $\hbar/\Delta E \sim 0.25$ ps, where \hbar is the reduced Planck constant. Even for this case, the mechanical time scale is two orders larger than the electron motion time scale, thus the deformation is still static from the electron's point of view.

Results. – To characterize the deformation of the graphene sheet, we use the ratio η between the maximum

²The contribution from the rotation of the p_z term is proportional to the vector product of the unit vector normal to the surface at an atom and the distance vector connecting it to its neighboring atoms. For small-amplitude vibration, these two vectors are approximately perpendicular to each other, thus the contribution would be small compared to the leading term.

deformation in the z -direction and the side length of the sheet (η_0 denotes the initial deformation). The maximum bond elongation occurred in our simulation is 9.46% when $\eta_0 = 0.09$, which is within the limits of experimental observation that the bond elongation can exceed 10% [34]. To gain insights, we first neglect nonlinear interactions so that the graphene sheet vibrates in its lowest mode, as shown in fig. 1(b), where each atom vibrates sinusoidally with amplitude determined by η_0 . A representative hopping-energy profile is shown in fig. 1(c) for $\eta = 0.07$.

Figure 2 shows, the time evolutions of the maximum deformation η (a), for two arbitrarily chosen Fermi energies, the transmission coefficients T (b), and (c) the Fourier transform of the transmission curves in (b). Since the deformation varies periodically, the hopping energies exhibit periodic variations, so does the transmission. However, since the hopping energies depend only on the amount of deformation (not on its direction), the frequency of variation in the hopping energies and transmission is twice that of the mechanical vibration. This is very clear in fig. 2(c), where the minimum dominant frequency in the Fourier spectrum is $2/T_0$ and T_0 is the period of the mechanical vibration. Note that in general T_0 depends on the shape of the flake, and also depends on which eigenmode the perturbation is. We also see that the transmission evolution exhibits relatively sharp changes (fig. 2(b)) instead of smooth variations as would be naively expected in view of the smooth and small-amplitude variations in mechanical deformations and hopping energies. The origin of the sharp fluctuations in the transmission can be understood as follows. As the graphene sheet deforms, the C-C bond is elongated, resulting in a smaller and position-dependent hopping energy. The variation in the hopping energies can be effectively characterized as the result of a local magnetic field [11], and electrons transporting through the deformed graphene sheet are scattered by this local field. As the amount of the deformation varies, so does the local field. At a certain point, the transmission can change drastically due to anomalous scattering. This is consistent with the previous finding that the transmission curve exhibits dramatic, fine-scale fluctuations *vs.* gradual variation of the potential barriers in a graphene quantum point contact, a relativistic quantum manifestation of Klein tunneling [35]. A direct consequence is that, because of the sharp transmission fluctuations, spurious higher-frequency components can emerge in the current through the device. For example, for $E/t_0 = 0.6525$, the first dominant frequency in the Fourier spectrum of the transmission is at $4/T_0$ (fig. 2(c)), instead of $2/T_0$. There are many such cases. And we have also observed that for some energies the first dominant frequency of the Fourier spectrum can be even at $6/T_0$.

To obtain a comprehensive picture of the behaviors of the transmission, we present the contour plot of the transmission *vs.* time and Fermi energy for the whole energy range $[0, t_0]$ for $\eta_0 = 0.07$, as shown in fig. 3(a). There is a wave-like pattern in time with exceptions at certain

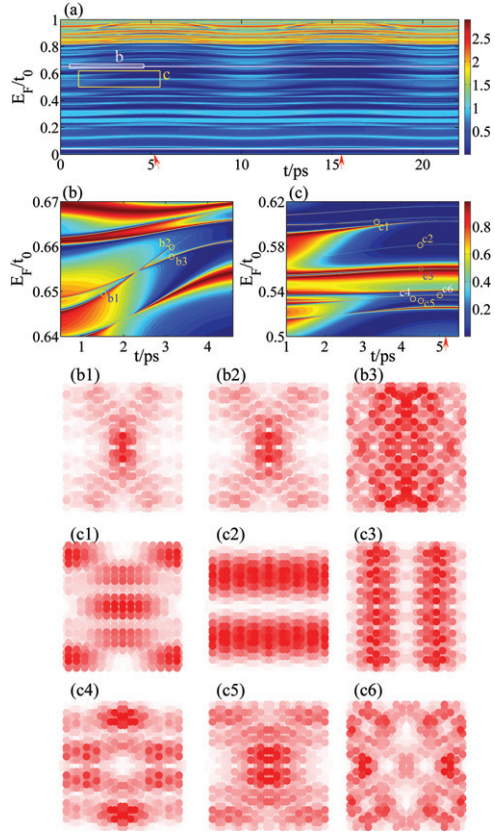


Fig. 3: (Color online) (a) Transmission *vs.* time and Fermi energy for the energy range of $[0, t_0]$. The white rectangles indicate the region of zoom-in in (b) and (c), where the white horizontal lines at $E/t_0 = 0.04$ and 0.6525 indicate the position of the transmission curves shown in fig. 2(b). The arrows in (a) and (c) indicate the time when the deformation amount returns to zero, and the first time instant for zero deformation is 5.16 ps. The initial deformation is $\eta_0 = 0.07$. The LDS patterns labeled (b1)–(b3) are for energies and time instances marked by the circles in (b), and the LDS patterns labeled (c1)–(c6) are marked by the circles in (c). Red (or dark grey) means high value of LDS.

points. The reason for this feature is the following. When calculating the transmission, the ratio E/t , where t is the hopping energy, is a key parameter. Although the hopping energy is position dependent, it decreases everywhere with deformation. In order to maintain the ratio, the corresponding global Fermi energy E needs to be smaller. The arrows in fig. 3(a) indicate the time when the deformation approaches zero. Starting from this point, as the deformation becomes progressively larger (by either going forward or backward in time), to keep the transmission unchanged (the same color scale or the contour line), the global Fermi energy needs to be reduced, thus the pattern bends down in the figure, forming the wave-like pattern. Besides the wave-like patterns, there are new features caused by anomalous scattering from the effective local fields. From fig. 3(b) and (c), we see that, as the deformation changes gradually, the transmission band

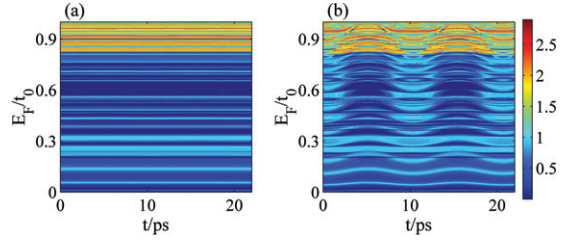


Fig. 4: (Color online) Contours of transmission in time and Fermi energy for initial deformations $\eta_0 = 0.01$ (a) and 0.09 (b), the maximum bond elongation at $t = 0$ is 1.09% and 9.46% , respectively.

varies accordingly. Furthermore, different bands change with different rates, leading to band crossings. Although some bands are dispersive with a finite width, there are finer structures in the bands of small energy or time (deformation) scales, implying the occurrence of a series of sharp electronic resonances.

To understand the mechanism of sharp resonances, we examine the local density of states (LDS) as the graphene sheet vibrates. We observe that, the LDS varies gradually but exhibits drastic changes occasionally, resulting in sharp resonances in the transmission curve. To unveil the formation of the narrow band structure, we analyze some typical LDS patterns (the lower panels in fig. 3) for the selected transmission bands shown in fig. 3(b), (c). We find that, for the transmission peaks in a single band, the LDS patterns are essentially identical (fig. 3(b1), (b2)), but they are characteristically different from those in the surrounding region or in a different band (fig. 3(b3)). From the typical LDS patterns it can be seen that the patterns for the narrow bands all correspond to strongly localized states [36–38] whose occurrence requires a fine match between the Fermi energy and the deformation amount. This gives rise to the sharp transmission peaks.

Another feature is that the transmission peak is broadened in energy when deformation presents compared with the case of zero deformation. This can be understood by considering the case of a sharp transmission peak *vs.* energy when there is no deformation. For small deformation, there is a spread in the hopping energies for different C-C bonds. Accordingly, due to the inhomogeneity of the distribution of the hopping energies, the Fermi energy required to maintain the transmission is broadened. A consequence is that the region of high transmission values is increased, leaving voids in the transmission plane at time instances with little deformation. For example, in fig. 3(a), for $t = 5.16$ ps there is no deformation. In this case, for $E_F/t_0 \in [0.4, 0.8]$, the transmission is mostly zero with some sharp transmission peaks. However, for $t = 0$ or 10.32 ps, the graphene sheet is maximally deformed, with the broadened transmission bands, the transmission is significantly enhanced, *e.g.* with more energy values that have large transmission. This can be better visualized in fig. 3(b), (c).

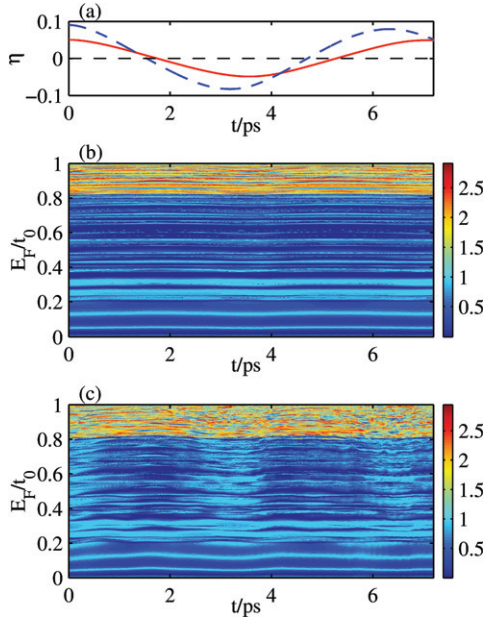


Fig. 5: (Color online) (a) Evolution of η with time for $\eta_0 = 0.05$ (solid curve) and 0.09 (dashed curve). (b), (c): transmission contours in time and Fermi energy for initial deformation $\eta_0 = 0.05$ and 0.09 , the corresponding maximum bond elongation at $t = 0$ is 5.36% and 9.46% , respectively.

We next examine the effect of the magnitude of the deformation. Figure 4 shows the transmission *vs.* time and Fermi energy for initial deformation amount $\eta_0 = 0.01$ and 0.09 . For $\eta_0 = 0.01$, the graphene sheet vibrates with a small amplitude, so do the hopping energies, leading to transmission that is nearly constant with time (fig. 4(a)). Note that for zero deformation, especially for Fermi energies below $0.8t_0$, the transmission peak is very narrow, thus for most energies the transmission is small, as indicated by the dominant dark-blue region in fig. 4(a) and fig. 4(b) at 5.16 ps . For $\eta_0 = 0.09$, at $t = 0$ or 10.32 ps , the graphene dot has the maximum deformation, each transmission peak at zero deformation becomes significantly broadened, thus for most energies the transmission becomes large, as indicated by the light-blue regions in fig. 4(b) at $t = 0$ or 10.32 ps . Therefore, the transmission is enhanced by mechanical vibration. However, for even larger deformation, the region of transmission plateaus can be greatly suppressed at the maximum deformation.

The results obtained so far are based on the linear term in the potential for mechanical vibrations and the initial deformation is with respect to the lowest eigenmode. In this approximation, the oscillation period of the graphene sheet is invariant for different deformation amplitudes. At $t = nt_0$, where n is an integer and $t_0 = 5.16\text{ ps}$, the graphene sheet becomes flat for odd n values and maximum deformation occurs for even n values, regardless of the deformation amplitude. When nonlinear terms are incorporated, the vibrational dynamics become quite intricate, resulting in complicated transmission patterns. For

relatively large deformation, the vibrations are no longer exactly periodic, but are approximately periodic with fine structures due to the diffusion of energy from the perturbed mode (the lowest) to high-frequency modes. The approximate period tends to decrease as the deformation amplitude is increased, as can be seen from fig. 5(a). Due to the excitation of higher modes, the largest displacement is no longer a smooth variable, so here η is the projection of the deformation profile to the first mode normalized by η_0 . Figure 5(b) shows the transmission contours in time and Fermi energy for $\eta_0 = 0.05$. As compared with the linear case, a distinct feature is the emergence of irregularity in time. In particular, in the linear regime a transmission peak for zero deformation is expanded into a band or a plateau in the plane of Fermi energy and time. However, in the nonlinear regime, the band or plateau is distorted. For a larger deformation, say, for $\eta_0 = 0.09$, because of the distorted deformation due to the excitation of high-frequency modes, different transmission bands merge to form nets that are more visible in the low energy range as the nets have larger energy and time scales (fig. 5(c)). Nevertheless, the enhancement of transmission in the presence of deformation is still clear, especially in the energy range $E_F/t_0 \in [0.4, 0.8]$. In this case, from the curve of transmission *vs.* time, one can estimate the period of the dominant lowest-frequency mode, but this period will become insignificant as more and more higher modes are excited.

Conclusion and discussions. – To summarize, we investigate electronic transport through rectangular graphene quantum dots where the graphene sheet is subject to periodic mechanical vibrations. We find that the quantum transmission coefficients exhibit periodic behaviors in time, providing an explanation for the time periodic variations in the currents of graphene-based nanoelectromechanical resonators. The transmission, however, contains more features besides the periodic variations. For small vibrational amplitude, the local maxima and minima in the curve of transmission *vs.* the Fermi energy are broadened to bands and plateaus in the two-dimensional plot of transmission *vs.* Fermi energy and time (deformation), leading to transmission enhancement. For large deformation amplitude, within a time period, resonant scattering can occur, leading to sharp fluctuations in the transmission. With nonlinear interactions, the mechanical motion becomes complex, giving rise to more complex transmission patterns such as nets from intertwined transmission bands, which can potentially result in spurious higher-frequency modes in the current. The complex transport behaviors uncovered provide insights into the interplay between mechanical and electronic properties of graphene in general. Note that so far we have considered perfect situations without any disorder. Due to the constraints of nanofabrication, there would exist a degree of strain inhomogeneity which could translate into randomness in the hopping energies beyond the changes induced

by the oscillation. However, from our results (figs. 3–5), insofar as the randomness in the bond elongation is small, say, a few percent, the main results should be unchanged, although the details of the transmission pattern can be different. If the randomness is large, *e.g.*, exceeding 5%, then the results could be altered.

This work was supported by NSF of China under Grants No. 11135001, No. 11375074 and No. 11422541, and by Doctoral Fund of Ministry of Education of China under Grant No. 20130211110008. YCL was supported by AFOSR under Grant No. FA9550-15-1-0151.

REFERENCES

- [1] CASTRO NETO A. H., GUINEA F., PERES N. M. R., NOVOSELOV K. S. and GEIM A. K., *Rev. Mod. Phys.*, **81** (2009) 109.
- [2] PERES N. M. R., *Rev. Mod. Phys.*, **82** (2010) 2673.
- [3] DAS SARMA S., ADAM S., HWANG E. H. and ROSSI E., *Rev. Mod. Phys.*, **83** (2011) 407.
- [4] HUANG L., XU H.-Y., LAI Y.-C. and CELSO G., *Chin. Phys. B*, **23** (2014) 070507.
- [5] LEE C., WEI X., KYSAR J. W. and HONE J., *Science*, **321** (2008) 385.
- [6] BUNCH J. S., VAN DER ZANDE A. M., VERBRIDGE S. S., FRANK I. W., TANENBAUM D. M., PARPIA J. M., CRAIGHEAD H. G. and MCEUEN P. L., *Science*, **315** (2007) 490.
- [7] BARTON R. A., ILIC B., VAN DER ZANDE A. M., WHITNEY W. S., MCEUEN P. L., PARPIA J. M. and CRAIGHEAD H. G., *Nano Lett.*, **11** (2011) 1232.
- [8] CHEN C., ROSENBLATT S., BOLOTIN K. I., KALB W., KIM P., KYMISSIS I., STORMER H. L., HEINZ T. F. and HONE J., *Nat. Nanotechnol.*, **4** (2009) 861.
- [9] XU Y., CHEN C., DESHPANDE V. V., DiRENNO F. A., GONDARENKO A., HEINZ D. B., LIU S., KIM P. and HONE J., *Appl. Phys. Lett.*, **97** (2010) 243111.
- [10] EICHLER A., MOSER J., CHASTE J., ZDROJEK M., WILSON-RAE I. and BACHTOLD A., *Nat. Nanotechnol.*, **6** (2011) 339.
- [11] GUINEA F., HOROVITZ B. and LE DOUSSAL P., *Phys. Rev. B*, **77** (2008) 205421.
- [12] DE PARGA A. V., CALLEJA F., BORCA B., PASSEGHI M. jr., HINAREJOS J., GUINEA F. and MIRANDA R., *Phys. Rev. Lett.*, **100** (2008) 056807.
- [13] KATSNELSON M. and GEIM A., *Philos. Trans. A Math. Phys. Eng. Sci.*, **366** (2008) 195.
- [14] LEVY N., BURKE S., MEAKER K., PANLASIGUI M., ZETTL A., GUINEA F., NETO A. C. and CROMMIE M., *Science*, **329** (2010) 544.
- [15] ZHANG D.-B., SEIFERT G. and CHANG K., *Phys. Rev. Lett.*, **112** (2014) 096805.
- [16] JISHI R., DRESSELHAUS M. and DRESSELHAUS G., *Phys. Rev. B*, **48** (1993) 11385.
- [17] YAN J., ZHANG Y., KIM P. and PINCZUK A., *Phys. Rev. Lett.*, **98** (2007) 166802.
- [18] PEREBEINOS V. and AVOURIS P., *Phys. Rev. B*, **81** (2010) 195442.
- [19] SHENOY V. B., REDDY C. D., RAMASUBRAMANIAM A. and ZHANG Y. W., *Phys. Rev. Lett.*, **101** (2008) 245501.
- [20] HUANG B., LIU M., SU N., WU J., DUAN W., GU B.-L. and LIU F., *Phys. Rev. Lett.*, **102** (2009) 166404.
- [21] ERIKSSON A. M., MIDTVEDT D., CROY A. and ISACSSON A., *Nanotechnology*, **24** (2013) 395702.
- [22] CHANG W.-J. and LEE H.-L., *J. Appl. Phys.*, **116** (2014).
- [23] LOBO C. and LUÍS J., *Z. Phys. D*, **39** (1997) 159.
- [24] KEATING P. N., *Phys. Rev.*, **145** (1966) 637.
- [25] MARTIN R. M., *Phys. Rev. B*, **1** (1970) 4005.
- [26] ATALAYA J., ISACSSON A. and KINARET J. M., *Nano Lett.*, **8** (2008) 4196.
- [27] PEREIRA V. M., NETO A. C. and PERES N., *Phys. Rev. B*, **80** (2009) 045401.
- [28] RIBEIRO R., PEREIRA V. M., PERES N., BRIDDON P. and NETO A. C., *New J. Phys.*, **11** (2009) 115002.
- [29] CARRILLO-BASTOS R., FARIA D., LATGÉ A., MIRELES F. and SANDLER N., *Phys. Rev. B*, **90** (2014) 041411(R).
- [30] BAHAMON D. A., QI Z., PARK H. S., PEREIRA V. M. and CAMPBELL D. K., *Nanoscale*, **7** (2015) 15300.
- [31] QI Z., KITT A. L., PARK H. S., PEREIRA V. M., CAMPBELL D. K. and CASTRO NETO A. H., *Phys. Rev. B*, **90** (2014) 125419.
- [32] DATTA S., *Electronic Transport in Mesoscopic Systems* (Cambridge University Press) 1995.
- [33] HUANG L., LAI Y.-C., FERRY D. K., AKIS R. and GOODNICK S. M., *J. Phys.: Condens. Matter*, **21** (2009) 344203.
- [34] LU J., NETO A. C. and LOH K. P., *Nat. Commun.*, **3** (2012) 823.
- [35] YANG R., HUANG L., LAI Y.-C. and GREBOGI C., *Phys. Rev. B*, **84** (2011) 035426.
- [36] AKIS R., FERRY D. K. and BIRD J. P., *Phys. Rev. Lett.*, **79** (1997) 123.
- [37] YOON Y., KANG M.-G., MORIMOTO T., KIDA M., AOKI N., RENO J. L., OCHIAI Y., MOUROKH L., FRANSSON J. and BIRD J. P., *Phys. Rev. X*, **2** (2012) 021003.
- [38] HUANG L., LAI Y.-C., LUO H.-G. and GREBOGI C., *AIP Adv.*, **5** (2015) 017137.